Risk-aware sizing and transactive control of building portfolios with thermal energy storage

Min Gyung Yu[a,1,*], Gregory S. Pavlak[a,1,2]

[a] *The Pennsylvania State University, 104 Engineering Unit A, University Park, PA 16802, USA*

Abstract

With the increasing numbers of distributed energy resources are being installed at more distributed locations, it is challenging to operate the electric grid systems efficiently against the demand and supply fluctuations. Moreover, extreme conditions could result in high expenditure and grid unreliability. To address this issue, this work focused on developing a risk-averse stochastic optimal dispatch model for building portfolios with thermal energy storage using conditional value at risk to avoid expected expensive financial loss at the tail of cost distribution. Two simulation case studies were performed to assess the performance of the risk-averse controller depending on the TES sizing and quantify the value of the proposed framework compared to the deterministic approach. The results demonstrated that the risk-averse controller could benefit from larger TES sizing as storing excess energy for the emergent realizations. Overall, 42.4% of cost savings was achieved by applying the risk-averse control strategy.

Keywords: conditional value at risk, demand response, transactive control, stochastic optimization, thermal energy storage

1. Introduction

There is a clear national and global trend toward a zero-carbon future with clean energy-related policies and low-priced renewable energy in the power markets. The original grid, which was built for one-way power flow from centralized power plants, has been transitioning to the smart grid with increased communication and distributed energy resources (DERs) to help reduce carbon emissions and increase local resilience. Accordingly, buildings are becoming electricity prosumers as they do not just consume energy for building demands, but also produce energy from distributed energy resources such as solar photovoltaic (PV) panels.

The grid-interactive efficient building (GEB) concept has been introduced to describe buildings with advanced controls to respond to grid pricing signals for building energy management as well as grid reliability. GEBs may utilize energy storage, distributed energy generation, and flexible load technologies, such as electric vehicles and intelligent controls. GEBs can help mitigate both peaks and valleys in net demand through enhanced coordination between energy supply and demand across the grid. Emerging grid-integrative buildings are expected to increase grid performance and better utilize renewable energy. However, it is challenging for the electric grid operators and building operators to make perfect decisions taking into account informational uncertainty and risk, since increasing numbers of DERs are being installed on the grid at more distributed locations.

Additionally, demand fluctuations due to occupant behavior and customers' engagement have been noted as the main uncertainties in demand response and energy management [1, 2]. The influence of weather changes has also been considered as a crucial source that may cause both unexpected load scenarios and

*Corresponding author

Email addresses: mzy57@psu.edu (Min Gyung Yu), gxp93@psu.edu (Gregory S. Pavlak)

[1] Department of Architectural Engineering

[2] Penn State Institutes of Energy and the Environment

Preprint submitted to : [Draft - Not for Distribution]

power price fluctuations [3, 4, 5]. Even though some extreme conditions may have a very low probability, they could result in a high impact on energy costs [6]. To deal with issues regarding decision-making under uncertainty and risk in grid-integrative building controls, this work proposes a risk-averse transactive control framework based on a stochastic optimization at the aggregator level for participating loads. This research extends our previous work which developed an uncertainty-aware transactive control framework based on two-stage stochastic optimization, and identified that the controller let to improved performance but was unable to adequately contend with low probability, high impact scenarios [7, 8]. Moreover, this work explored the relationship between the control strategies and the optimal sizing of the thermal energy storage assets to maximize the benefits of the proposed risk-aware control framework.

This paper is organized as follows: In Section 2, studies on grid integrated operation to address uncertainties are described. In Section 3, the architecture of the uncertainty- and risk- aware control platform is illustrated. The mathematical formulation for risk-averse stochastic optimization problem is presented in Section 5. Case studies and results are highlighted in Section 6. Finally, the conclusions and discussion are presented in Section 7.

2. Prior research, gaps, and motivation

It becomes more important to consider uncertainties and risks when it comes to making energy procurement and management decisions in the context of the future grid with high renewables and DERs. Many researchers have examined risk factors for reliable energy management and reduction of financial loss from the risks [9, 10]. In power grids, supply and demand fluctuations, development of technology, political plans, price variability, and participation were considered as the main risks that could affect grid deployment and operations [2, 11].

Modeling approaches for grid electric operation and scheduling to robustly deal with problems of weather-related uncertainties have been proposed and have demonstrated less sensitivity to climate uncertainty while maintaining high-performance [6, 12]. Previous research also found that a method to handle both typical and extreme weather conditions provided more reliable performance benefits [13].

Many researchers have applied risk measurement analysis to estimate the impact from the risks and develop risk-based energy management to increase the resilience of the power grid operation [14, 15, 16, 17]. Different risk measures, such as variance, value-at-risk (VaR), and conditiona value-at-risk (CVaR) were introduced to handle the risks in stochastic programming. Yin et al. proposed risk-aware energy optimization models considering uncertain wind, sky, and dust conditions [18]. They suggested adding production variance risk (PVR) to specify a control threshold by bounding the variance of energy production below a risk level or utilizing production percentile risk (PPR) to avoid the undesired situation where the energy production falls below a threshold. They demonstrated the performance of the models with a large hybrid wind-solar farm. Ali et al. developed a risk-constrained framework to optimize the operation of space heating load to minimize the user expected payment while restricting the financial risk imposed by uncertain power prices and stochastic heat demand to a certain level [19]. They adopted a mean-variance approach which denotes the volatility with the standard deviation of the cost at different scenarios, and the result demonstrated the framework to be implemented at the household level. Tian et al. researched risk-involved scheduling for an aggregator of plug-in electric vehicles based on day-ahead and reserve markets using the downside risk constraints method. Downside risk constraints based on market price scenarios were utilized to provide decisions considering various quantities for risk [20]. VaR and CVaR have been widely utilized by assigning a probability to risk events and predicting the possibility of a future outcome. VaR is a technique broadly utilized in financial risk assessment and electricity risk management but it cannot indicate the potential losses exceeds the VaR. On the other hand, CVaR which is derived from VaR estimates the expectation of financial loss, thus, it is a stable calculation over VaR. The simple mathematical methodology has been applied to energy management for buildings [21, 22, 23, 24, 25], energy hub [26, 27, 28], renewable energy systems [29], EV aggregators [30, 31], grid operator [32, 33, 34, 35], retailers [36], and a demand response aggregator [37]. However, there is little research developing a methodology that can mitigate these risks at an aggregator level integrating building customers' thermal energy storage assets.

To highlight the performance of risk-aware energy management, previous research classified the aggregators into risk-neutral, risk-averse, and risk-taking [33]. The risk-averse aggregator operates to avoid the risk , while the risk-taking aggregator commits at a higher risk level[32]. Results show that risk-taking market players help to further flatten the load profile of the system, which enhances the efficiency of the market operation however the higher risk-takers may face a loss instead of making a profit at the same time [23]. Previous research demonstrated the effectiveness of risk-constrained operators, however, they did not consider the relationship between the operating strategies and the capacity of flexible energy resources [22].

Based on the literature review, recent research has studied the risk-aware scheduling for electric grid operation. However, no previous studies have developed risk-aware scheduling for an aggregator of multiple buildings with thermal energy storage resources. In addition to that, there is little research study on how appetite for risk may influence energy system design perspectives. Thus, more research is needed to understand the performance of a large-scale portfolio with building thermal energy storage depending on the aggregator's tolerance for risk.

To address these needs, this work aims to propose an uncertainty- and risk-aware transactive control framework for building portfolios with thermal energy storage systems. This research can quantify the undesirable risks from occupant behavior, renewable energy generation, weather conditions, and electricity prices. Through our research, a risk-averse stochastic optimization model for an aggregator of building thermal energy resources can mitigate financial risk and achieve higher benefits for both aggregator and customers. On top of that, the optimal sizing of thermal energy storage can be recommended based on the risk preferences of the aggregator. Thus, the primary contributions of this work are:

- A risk-averse two-stage stochastic formulation for both day-ahead energy procurement and real-time dispatch of building thermal storage assets.
- A quantification of the supervisory controller value depending on the level of risk-aversion and varying building loads.
- Optimal sizing of flexible energy resources related to the energy control strategies.

This study provides insights into the supervisory controller related to risk in demand flexibility for building-based grid services. This study will enable the microgrid operator or aggregator to select desirable risk-taking capabilities.

3. Uncertainty- and risk-aware transactive building energy control framework

Figure 1 highlights the architecture of uncertainty- and risk-aware transactive energy control framework for an aggregator of multiple buildings. The aggregator has two main tasks which are day-ahead power procurement and real-time power dispatch to the building customers. First, the aggregator determines how much power to procure in the day-ahead market for the following days via a two-stage stochastic optimization. The power procurement decision is made to minimize the total cost of procurement and expected real-time balancing costs. In day-ahead, the expected real-time balancing cost is estimated over a set of uncertain scenarios with building load, power prices, weather, and PV power generation.

In real-time, the optimal power is dispatched to multiple buildings with a stochastic MPC. Based on the day-ahead power procurement decision, the aggregator may need to purchase additional energy from the real-time balancing market for the required building demand or it can sell excesss power for its profits. The framework enables the aggregator to maximize its profits (and corresponding the value to all participants) by integrating the building customers' thermal energy storage operation. The transactive control mechanism is introduced here to provide demand response (DR) incentives to customers controlling the operation of thermal energy storage systems according to the aggregator's direction.

Figure 2 illustrates the detailed transactive market model of this work. Each building submits its own transactive response curve representing its preference on flexibility and operational constraints. Then, the aggregator clears the market price according to the actual real-time grid signals and the building receives the control signal related to the cleared price. For example, the aggregator can direct to reduce the building

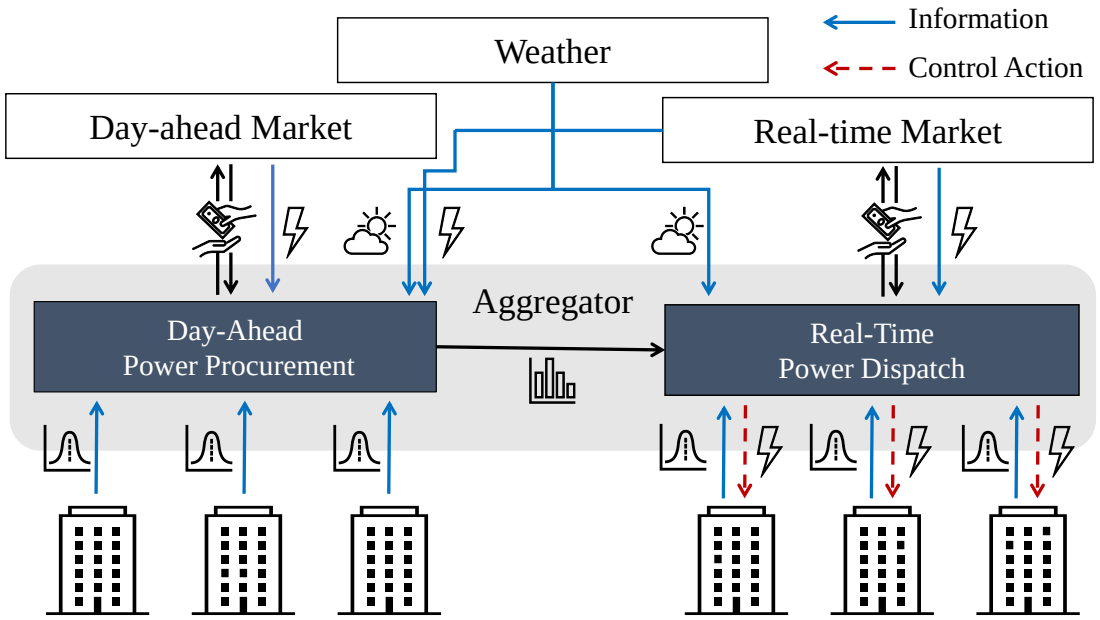

Figure 1: Architecture of the uncertainty- and risk- aware transactive building energy control platform.

load by discharging the TES when the pricing signals are high, while it can increase the building load by charging the TES when the power prices are low. The customers can get reimbursement by the amount of flexible response they provide. The mathematical formulation of the transactive power and modulated building demand is expressed as Eq. (1) - (3),

$$\delta_{b,t} = \theta_b \lambda_t^{cl} \tag{1}$$

$$q_{b,t}^k = q_{b,t} + \delta_{b,t} COP_b \tag{2}$$

$$p_b^k = q_{b,t}^k / COP_b + p_b^{oth} \tag{3}$$

The power compensation $\delta_{b,t}$ is estimated with the cleared market price λ_t^{cl} and customer preference θ_b as in Eq. (1). By controlling the operation of thermal energy storage, the total heat transfer rate of plant system is modified from $q_{b,t}$ to $q_{b,t}^k$. The amount of modulated heat transfer rate is calculated by converting the power compensation $\delta_{b,t}$ with the coefficient of the system (COP), which defines how much power is consumed to produce the heat as in Eq. (2). In reality, the energy system has non-linear operating characteristics, however, this work applied constant COP for the total cooling plant system to reduce computational burden in the control problem [38]. To simulate operating a real building, a detailed physics-based building model was utilized to make up for the performance differences. The modified building electric demand $p_{b,t}^k$ is the power consumed for the modified heat transfer rate $q_{b,t}^k$ and other electrical loads from light and electric equipment $p_{b,t}^{oth}$ as in Eq. (3).

4. Uncertainty quantification

The uncertainty modeling is important for stochastic control problems to obtain meaningful optimal solutions. The main uncertainties in the proposed framework are building loads (thermal and electric), power prices, weather conditions, and PV power generation. In this work, a vector autoregression (VAR) model was developed for forecasting scenarios to capture the relationship among the uncertainties [39]. Like the autoregressive (AR) model, each variable has a regression equation by observing the lagged values of

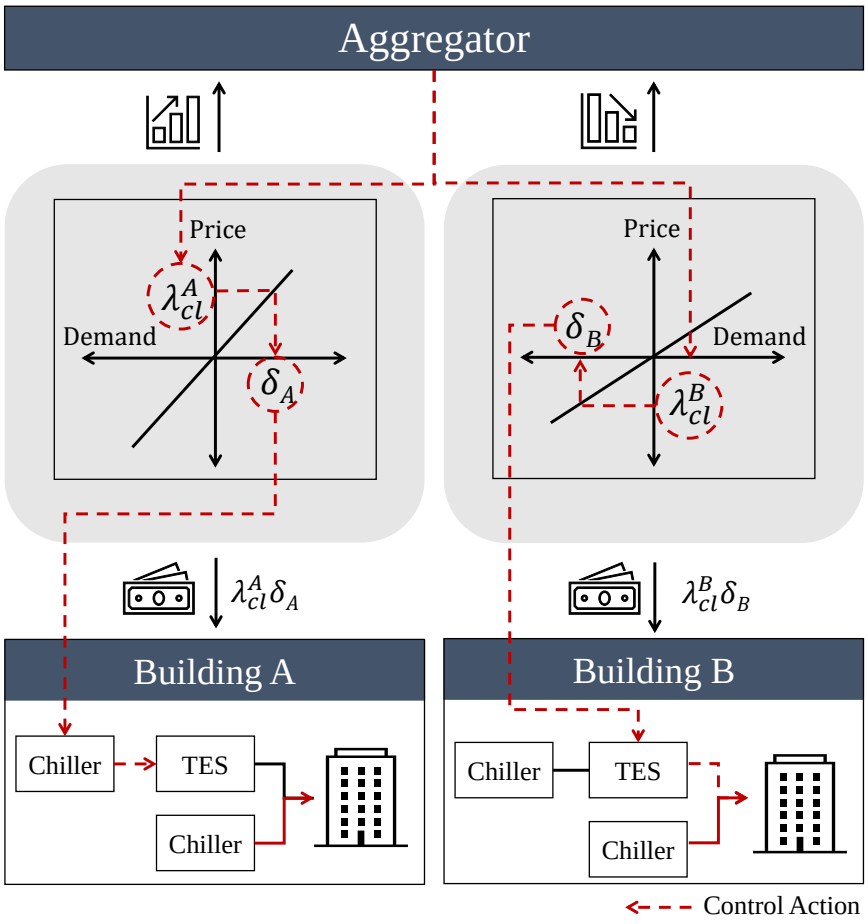

Figure 2: Transactive market model of this work.

all variables in the model. VAR models assumes that the variables are stationary, thus, the data was pre-processed using differencing to remove any trends and seasonal effects. This work applied the `statsmodels` package in Python to model the VAR. The VAR model produces forecasts, computes forecast covariance matrices, and constructs forecast interval estimates [40]. Accordingly, the stochastic model generates a set of scenarios based on the forecasting outputs. Two weeks of historical data weree used to generate the VAR model in this work, and the day-ahead power procurement problem uses a 24-hour period for the forecasts. The time-series forecasting model for day-ahead planning was developed, and the mean value and forecast interval estimates are obtained with the forecast model. The stochastic forecast scenarios are generated using Monte Carlo sampling. In the real-time model predictive controller, the VAR model was updated at every time interval with the newly observed data to generate a new set of scenarios. A normal distribution was utilized to get the stochastic scenarios for outdoor air temperature and real-time power prices. The stochastic scenarios for building demands and PV generation were generated based on the truncated normal distribution to constrain the sampled values to be positive.

5. Computational framework

In this section, we present a risk-aware stochastic programming model for day-ahead planning. After, we conclude with a risk-aware stochastic MPC problem for real-time operation.

5.1. Risk-neutral day-ahead stochastic power procurement model

In the previous research [8], we formulated the day-ahead power procurement problem as a two-stage stochastic optimization with the intent of minimizing electricity procurement cost and expected real-time operation cost, as defined in Eq. (4).

$$\min \quad c^T \mathbf{x} + \mathbb{E}\left[\mathcal{Q}(\mathbf{x}, \omega)\right] \tag{4}$$

$$\text{subject to} \quad 0 \leq \mathbf{x} \leq \sum_{b \in B} p_b^h, \tag{5}$$

where $c \triangleq \lambda^{\mathrm{da}}$ is the vector of day-ahead prices and p_b^h represents the peak electric demand of historical data. This planning problem is solved subject to a constraint in the first stage as in Eq. (5). The second-stage objective function $\mathcal{Q}(\mathbf{x}, \omega)$ is defined as the optimal value of the second-stage problem which is related to the real-time operation cost. We will describe it in more detail in the following section 5.2.

5.2. Risk-averse day-ahead stochastic power procurement model

The earlier model is a risk-neutral framework. This can be recast as a risk-averse framework by using the CVaR to capture the tail risk. For a confidence level β, the conditional value-at-risk is defined as Eq. (6).

$$CVaR_\beta(\mathcal{Q}(\mathbf{x}, \omega)) = \min_m \left(m + \frac{1}{1-\beta} \mathbb{E}\left[\mathcal{Q}(\mathbf{x}, \omega) - m\right]^+ \right) \tag{6}$$

where m is the VaR_β, and $[\mathcal{Q}(\mathbf{x}, \omega) - m]^+$ indicates the positive elements.

We assumed that the second-stage objective $\mathcal{Q}(\mathbf{x}, \omega)$ of the risk-neutral framework is the loss associated with a set of first stage decision variables $\mathbf{x}$ and the random variable ω. Then the objective of risk-averse stochastic dispatch is formulated as Eqs. (7)–(10) as noted in Wan [41].

$$\min_{\mathbf{x}} \left(c^T \mathbf{x} + CVaR_\beta\left(\mathcal{Q}(\mathbf{x}, \omega)\right) \right) \tag{7}$$

$$= \min_{\mathbf{x}} \left(c^T \mathbf{x} + \min_m \left(m + \frac{1}{1-\beta} \mathbb{E}\left[\mathcal{Q}(\mathbf{x}, \omega) - m\right]^+ \right) \right) \tag{8}$$

$$= \min_{\mathbf{x}, m} \left(c^T \mathbf{x} + m + \frac{1}{1-\beta} \mathbb{E}\left[\mathcal{Q}(\mathbf{x}, \omega) - m\right]^+ \right) \tag{9}$$

$$= \min_{\mathbf{x}, m} \left(c^T \mathbf{x} + \mathbb{E}\left[h\left(\mathcal{Q}(\mathbf{x}, \omega), m\right)\right] \right) \tag{10}$$

where

$$h\left(\mathcal{Q}(\mathbf{x}, \omega), m\right) = m + \frac{1}{1-\beta} \left[\mathcal{Q}(\mathbf{x}, \omega) - m\right]^+ \tag{11}$$

The risk-averse two-stage stochastic formulation consists of the first term for the day-ahead procurement costs and the second term for the conditional value-at-risk of the loss function $\mathcal{Q}(\mathbf{x}, \omega)$ over the set of stochastic scenarios Ω. Unlike the risk-neutral formulation in Eq. (4), the variables related to the first stage are the procurement decision $\mathbf{x}$ and value-at-risk m. The variables related to the second stage are related to the expected real-time operation which can be corrected when the actual realization is observed. The second stage problem is to minimize the conditional value-at-risk as in Eqs. (12) – (13).

$$h\left(\mathcal{Q}(\mathbf{x}, \omega), m\right) = \min \left(m + \frac{1}{1-\beta} \left[\mathcal{Q}(\mathbf{x}, \omega) - m\right]^+ \right) \tag{12}$$

$$= \min \left(m + \frac{S_\omega}{1-\beta} \right) \tag{13}$$

$$\text{subject to} \quad S_\omega \geq 0 \tag{14}$$

$$S_\omega \geq \mathcal{Q}(\mathbf{x}, \omega) - m \tag{15}$$

where S_ω is the dummy variable. Two constraints (14) – (15) are to constrain the dummy variable to be positive value of the deviation between the cost function $\mathcal{Q}(\mathbf{x}, \omega)$ and the value at risk m. The cost function $\mathcal{Q}(\mathbf{x}, \omega)$ represents the real-time operating cost as formulated in Eq. (16).

$$\begin{aligned}\mathcal{Q}(\mathbf{x}, \omega) = &\sum_{b \in B} \left((\lambda^{cl}_{b,\omega})^T \delta_{b,\omega} \right) + \lambda^{dr} \sum_{b \in B} z_{b,\omega} - \lambda^{ba} \mathbf{1}^T \sum_{b \in B} p^k_{b,\omega} + (\lambda^{rt}_\omega)^T (u^+_\omega - u^-_\omega) \\ &+ \eta_1 \|u^+_\omega\|^2 + \eta_1 \|u^-_\omega\|^2 + \eta_2 \sum_{b \in B} q^{ne}_{b,\omega} + \eta_3 \sum_{b \in B} q^{ov}_{b,\omega} + \eta_4 p^{ex}_\omega + \eta_5 (y^2_{1,\omega} + y^2_{2,\omega}) \end{aligned} \tag{16}$$

where λ^{dr} is the demand response price; λ^{ba} is the base price; λ^{rt}_ω is the vector real-time power price in scenario ω; $u^+_\omega, u^-_\omega, z_{b,\omega}, y_{1,\omega}, y_{2,\omega}$ are the dummy variables; η is the penalty value.

The first two terms in Eq. (16) represent the incentives that the aggregator provides to the customer for the demand flexibility, while the third term is the revenue of the aggregator by selling power to customers for their building demand. The fourth term is the balancing cost in the real-time power market and can be either profit or expenditure as purchasing or selling power. The scenario-specific real-time power prices are utilized for this cost. The fifth and sixth terms are penalties on the hourly deviation between actual power and the day-ahead procurement. The seventh term is a comfort penalty to check if the total thermal supply meets the thermal demand. The eight-term is a penalty on the extra discharging over the cooling demand. The ninth term is for the penalty over the peak demand limit. The tenth term is a penalty enforcing that the daily sum of procured energy is within ±25% of the total daily expected energy use. The cost function $\mathcal{Q}(\mathbf{x}, \omega)$ is defined over the set of stochastic scenarios Ω, and constrained by the system characteristics in real-time operation.

Overall, the complete set of second-stage objectives and constraints are formulated as in Eqs. (17) – (36), where $q^k_{b,\omega} = \left\{ q^k_{b,t,\omega} : \forall t \in T \right\}$ is the vector of the actual heat transfer rate to user side of building b in scenario w; $q_{b,\omega} = \left\{ q_{b,t,\omega} : \forall t \in T \right\}$ denotes the building cooling demand in scenario ω; $SOC_{b,\omega} = \left\{ SOC_{b,t,\omega} : \forall t \in T \right\}$ is the vector of the state-of-charge (SOC) levels of TES in scenario w; CAP^{tes}_b is the thermal energy storage capacity of the building b; CAP^{ch}_b is the capacity of the dedicated thermal energy storage chiller of the building b.

In this scheme, the building demand $q_{b,\omega}$ and the real-time power price λ^{rt}_ω are from the forecasting models, and these are different from the actual realizations in the real-time operation. We assumed that all the expected values $\mathcal{Q}(\mathbf{x}, \omega)$ have the same probabilities in this problem.

$$h\left(\mathcal{Q}(\mathbf{x},\omega),m\right) = \min\left(m + \frac{S_\omega}{1-\beta}\right) \tag{17}$$

$$\text{subject to} \quad S_\omega \geq 0 \tag{18}$$

$$\begin{aligned} S_\omega \geq & \sum_{b\in B}\left((\lambda^{cl}_{b,\omega})^T\delta_{b,\omega}\right) + \lambda^{dr}\sum_{b\in B} z_{b,\omega} - \lambda^{ba}\mathbf{1}^T\sum_{b\in B} p^k_{b,\omega} \\ & + (\lambda^{rt}_\omega)^T(u^+_\omega - u^-_\omega) + \eta_1\|u^+_\omega\|^2 + \eta_1\|u^-_\omega\|^2 + \eta_2\sum_{b\in B} q^{ne}_{b,\omega} \\ & + \eta_3\sum_{b\in B} q^{ov}_{b,\omega} + \eta_4 p^{ex}_\omega + \eta_5(y^2_{1,\omega} + y^2_{2,\omega}) - m \end{aligned} \tag{19}$$

$$p^k_{b,t,\omega} = q_{b,t,\omega}/COP + \delta_{b,t,\omega} + p^{oth}_{b,t,\omega} \quad \forall b,t \tag{20}$$

$$0, \pm\lambda^{cl}_{b,t,\omega} \leq z_{b,t,\omega}, \quad \forall b,t \tag{21}$$

$$0 \leq u^-_{t,\omega}, u^+_{t,\omega}, y_{1,\omega}, y_{2,\omega}, \quad \forall t \tag{22}$$

$$(u^+_{t,\omega} - u^-_{t,\omega}) = \sum_{b\in B} p^k_{b,t,\omega} - x_t, \quad \forall t \tag{23}$$

$$y_{1,\omega} - a_1\sum_{b\in B}\sum_{t\in T} p^k_{b,t,\omega} \leq \mathbf{1}^T\mathbf{x} \leq y_{2,\omega} + a_2\sum_{b\in B}\sum_{t\in T} p^k_{b,t,\omega} \tag{24}$$

$$SOC^{\min}_b \leq SOC_{b,t,\omega} \leq CAP^{\text{tes}}_b \quad \forall b,t \tag{25}$$

$$\delta_{b,t,\omega}COP_b = (SOC_{b,t,\omega} - SOC_{b,t-1,\omega})CAP^{\text{tes}}_b, \forall b,t \tag{26}$$

$$\delta_{b,t,\omega}COP_b \leq CAP^{ch}_b, \quad \forall b,t \tag{27}$$

$$\delta_{b,t,\omega}COP_b \leq (SOC^{\max}_b - SOC_{b,t,\omega})CAP^{tes}_b, \quad \forall b,t \tag{28}$$

$$(SOC^{min}_b - SOC_{b,t,\omega})CAP^{\text{tes}}_b \leq \delta_{b,t,\omega}COP_b, \quad \forall b,t \tag{29}$$

$$0 \leq p^k_{b,t,\omega}, \quad \forall b,t \tag{30}$$

$$q^{dis}_{b,t} \leq 0 \quad \forall b,t \tag{31}$$

$$q^{dis}_{b,t,\omega} \leq \delta_{b,t,\omega}COP_b, \quad \forall b,t \tag{32}$$

$$0 \leq q^{ne}_{b,t,\omega}, q^{ov}_{b,t,\omega}, p^{ex}_{t,\omega}, \quad \forall b,t \tag{33}$$

$$0 \leq \delta_{b,t,\omega}COP_b + q_{b,t,\omega} + q^{ov}_{b,t,\omega}, \quad \forall b,t \tag{34}$$

$$q^{dis}_{b,t,\omega} - CAP^{ch2}_b + q_{b,t} \leq q^{ne}_{b,t,\omega}, \quad \forall b,t \tag{35}$$

$$\sum_{b\in B} p^k_b - p^{ex}_{t,\omega} \leq p^{peak} \tag{36}$$

Description of constraints. Eqs. (18) – (19) constrain the dummy variables to be positive values to estimate CVaR. Eq. (20) represents the compensation determined by the transactive response curve while Eq. (21) defines z, which is the absolute value of the clearing price. Eq. (22) is to constrain the dummy variables to be positive. Eq. (23) denotes the deviation between the actual total building demand and the procurement. Eq. (24) constrains the daily sum of procured energy to be within ±25% of the total daily expected energy use in scenario ω, thus, a_1 and a_2 represent 1.25 and 0.75, respectively, in this work. Eq. (25) constrains the SOC levels of the TES within the specified range with lower and upper limits. Eq. (26) defines the SOC level of the TES in each time interval as calculated through the TES heat transfer rate to the user side or from the source side and building load. Eqs. (27)-(28) keep the maximum TES charging energy limit by the minimum of the dedicated TES chiller capacity and the extra heat capacity of TES. Eq. (29) restricts the maximum TES discharging rate by the rest of the thermal energy in TES. Eq. (30) defines the actual building electric demand should be positive. Eqs. (31)-(32) represent the TES discharging rate showing the negative value. Eq. (33) indicates the positive values for dummy variables. Eq. (34) constrains that the

discharging strategy can be above the cooling demand considering the other scenarios with a given penalty in the objective function. Eq. (35) defines thermal energy that does not meet the cooling demand with the TES discharging rate and the base chiller capacity as $q_{b,t}^{ne}$. Eq. (36) constrains the aggregated actual power to be below the peak limit.

5.3. Risk-averse real-time stochastic power dispatch model

In the real-time operation, the aggregator modulates the operation of multiple building TES with a model predictive controller. The risk-averse stochastic MPC can be also formulated by combining the risk-neutral stochastic MPC and CVaR. First, the risk-neutral two-stage MPC is formulated to minimize the sum of the operation costs at current time interval and the expected operation costs for the subsequent time intervals as in Eq. (37).

$$\min \quad f(x) + \mathbb{E}\left[f(x,\omega)\right] \tag{37}$$

The first term in Eq. (37) is the operation cost of the current time interval and the second term is the expected cost for the following time intervals. We assumed that the HVAC operator can control the systems following the actual building demand at the current time interval, thus, we used the perfect information for the first stage.

In the risk-averse real-time stochastic power dispatch model, the operation cost for the current time interval is formulated as referring to the cost function $\mathcal{Q}(\mathbf{x},\omega)$ in Eq. (16), and the perfect information is implemented instead of the uncertain scenario ω. The constraints are followed by Eqs. (20) – (36). The formulation of the operation cost for the subsequent time intervals is referred to Eq. (12) and constrained by Eqs. (18) – (36) over all scenarios ($\omega \in \Omega$). In addition, the penalty parameters η_1 and η_5 are set to zero to remove the constraints related to the power procurement decision. This work implemented the MPC problem with a fixed horizon of one day.

5.4. Optimal TES sizing coupled with stochastic optimization

To derive optimal sizing of TES, an additional integer variable for TES can be included in both risk-neutral and risk-averse stochastic models. For example, the risk-neutral stochastic optimization for the optimal TES sizing can be redefined as in Eq. (38). However, these changes would lead to bilinear terms with SOC and CAP_b^{tes}, which will add non-convexities and make it difficult to solve. Therefore, we redefined the state of charge of TES SOC, which initially ranged from 0 to 1, to instead directly represent the stored thermal energy (kWh) in the TES to avoid the bilinear terms in this section.

$$\min_{\mathbf{x}, CAP^{tes}} \quad (\lambda^{\mathrm{da}})^T \mathbf{x} + \mathbb{E}\left[\mathcal{Q}(\mathbf{x},\omega)\right] + \eta_0 \sum_{b\in B} CAP_b^{tes} \tag{38}$$

$$\text{subject to} \quad 0 \le \mathbf{x} \le \sum_{b\in B} p_b^h, \tag{39}$$

$$0 \le CAP_b^{tes}, \tag{40}$$

The third term of the objective function enforces that we would like the smallest TES size required, and Eq. (40) constrains the TES capacity to be positive. The constraints of the second stage problem are limited by first-stage decisions $\mathbf{x}$ and CAP_b^{tes}. Thus, the first stage will decide the capacity of thermal energy storage CAP_b^{tes} as well as the procurement decision $\mathbf{x}$. The following Eqs. (41) - (44) are the updated constraints in the second stage problem,

$$SOC_b^{\min} CAP_b^{\mathrm{tes}} \le SOC_{b,t,\omega} \le SOC_b^{\max} CAP_b^{\mathrm{tes}} \quad \forall b,t \tag{41}$$

$$\delta_{b,t,\omega} COP_b = (SOC_{b,t,\omega} - SOC_{b,t-1,\omega}), \forall b,t \tag{42}$$

$$\delta_{b,t,\omega} COP_b \le (SOC_b^{\max} CAP_b^{\mathrm{tes}} - SOC_{b,t,\omega}), \quad \forall b,t \tag{43}$$

$$(SOC_b^{min} CAP_b^{\mathrm{tes}} - SOC_{b,t,\omega}) \le \delta_{b,t,\omega} COP_b, \quad \forall b,t \tag{44}$$

where $SOC_{b,\omega} = \left\{SOC_{b,t,\omega} : \forall t \in T\right\}$ is the vector of the remaining thermal energy of TES in scenario ω.

Eq. (41) constrains thermal energy stored in the TES to be positive and lower than the capacity of the TES. Eq. (42) defines the thermal energy stored in the TES in each time interval as calculated through the TES heat transfer rate to the user side or from the source side and building load. Eq. (43) keeps the maximum TES charging energy limit to be lower than the extra heat capacity of TES. Eq. (44) restricts the maximum TES discharging rate by the rest of the thermal energy in TES.

6. Case Studies

Simulation case studies were carried out to evaluate the performance of the risk-averse stochastic controllers for building portfolios with TES.

The first simulation study, analyzes the risk-neutral and risk-averse controllers for three different building portfolios that have different TES sizes.

The second case study evaluates the performance of the portfolio when the TES is both sized and operated from uncertainty- and risk-aware perspectives. The optimal sizing of the TES system was determined by solving the day-ahead problem in Section 5.4. Within this study, the risk-neutral and risk-averse controllers are also compared to a deterministic reference case and a perfect information case. The deterministic model uses the mean value of the forecasting model in planning and operations, while the perfect information case uses the actual conditions.

The second simulation study also presents results for a portfolios of building customers with PV generation and a portfolio without PV to explore the capabilities of the proposed frameworks when more variability is present in the net electric load.

In this work, the aggregator's portfolio consists of three office buildings located in Chicago, IL. The building models were generated by varying the occupancy schedules and parameters of the reference model to create various realizations of the building demands. The detailed building information, including geometry and plant system configuration, is described in our previous research [7, 8]. The performance analysis focused on evaluating how the stochastic controller operates differently depending on the risk-aversion levels (e.g., risk-neutral vs. risk-averse) and assessing when we can benefit from the risk-averse stochastic controller. The stochastic problem contains 100 forecast scenarios for each building, thus, a total of 57,948 variables and 132,600 constraints were considered when solving the three-building portfolio problems. The simulations were run on a machine with 2.2 GHz Intel Xeon processors and 256 GB RAM. The scripts weree developed in Python and the optimization problems were solved using Mosek[42].

6.1. Case 1: Uncertainty and risk-aware transactive control of building TES portfolios

To initially explore the behavior and benefits of risk-averse control we present results for the risk-averse and risk-neutral controllers for building portfolios with three different TES sizes. Table 1 summarizes the results for aggregator using risk-neutral and risk-averse controllers in terms of operating costs, penalty charges, and total costs for one week (6/4 - 6/8). Figure 3 shows a one-day (June 5th) snapshot of the cost functions and actual power. The subfigures in the first row of Figure 3 show the comparison of actual power for both risk-neutral (blue solid line) and risk-averse (red solid line) with the original electric demand (grey dashed line). The subfigures in the second row of Figure 3 show the sum of operation costs (grey box) and peak penalty charges (white box with hatch) for both risk-neutral and risk-averse cases.

When TES capacity was high (i.e., 180 kWh), both cases reduced the peak demand by controlling TES operation, and the risk-averse strategy had the lowest penalty charges. Even though operating costs for risk-averse strategy were a bit higher than those for risk-neutral strategy, it could avoid the peak penalty and produce greater savings overall. The detailed cooling operations are illustrated in Figure 4 for the representative day (June 5th). As observed in Figure 4, the risk-averse case charged a large amount of energy during the early morning hours so that it could discharge thermal energy to reduce the peak demand. On the other hand, the risk-neutral case could not discharge at the end of operation due to the lack of stored energy in TES.

As we reduce the TES capacity from 180 kWh to 100 kWh, and then to 50 kWh, the control strategies for both risk-neutral and risk-averse became similar as observed in Figure 4. The difference in operating

Table 1: Comparison of the operating costs and penalty charges by control method and TES size.

Case		Operation ($)	Penalty ($)	Sum ($)
TES	Risk-neutral	18.3	1.8	20.1
180 kWh	Risk-averse	18.9	0.9	19.8
TES	Risk-neutral	17.0	2.8	19.8
100 kWh	Risk-averse	17.7	2.7	20.4
TES	Risk-neutral	17.2	5.5	22.7
50 kWh	Risk-averse	17.2	5.7	22.9

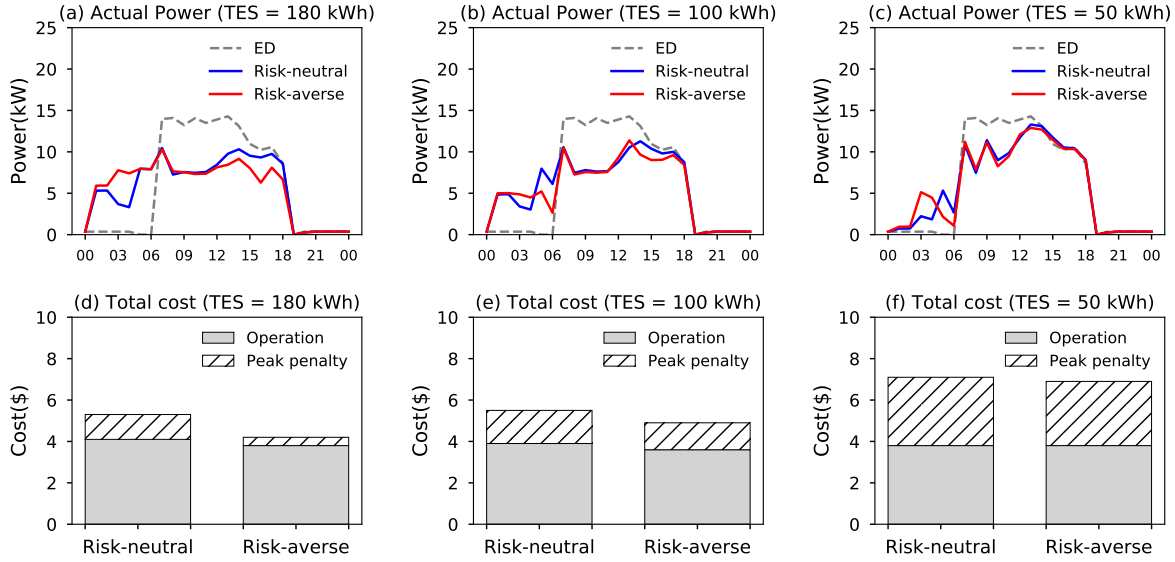

Figure 3: Comparison of RT actual power and total costs (June 5th).

between Figure 4(a) and (c) was relatively large, while the operating characteristics between Figure 4(b) and (d) were close. Both did not perform well with the smallest TES capacity (i.e., 50 kWh) when the actual demand was much higher. Accordingly, the peak penalty charges increased by 3 to 5 times. We also observed that the risk-averse stochastic controller tends to charge when it is possible to use for emergency cases. However, it could not benefit from taking into account the tail values as it is not capable to save extra energy due to small TES sizing. Overall, it was determined that the capabilities of risk-averse strategy can be highly related to the TES capacity, and the benefits can be maximized when a large enough TES size is installed. In other words, if we want to realize the benefits of the risk-aware framework to guard against costly extremes, the system must be designed considering the optimal recourse needed during these extreme scenarios. This observation motivated the extension to coupled risk-averse sizing and dispatch, and the results are presented in the following section.

6.2. Case 2: Risk-averse sizing and TES dispatch

To optimize the size of the TES in the building portfolios we first solved Eq. (38) for each day of the operating period assuming the TES started with a SOC of zero. The largest required TES size among the daily operations was selected and the optimal TES size. Once the required size was determined, the value was fixed and the portfolios were re-optimized to determine the actual operating costs over the simulation period. In the subsections below, results are presented for both the building portfolios with PV generation and a building portfolio without PV generation included.

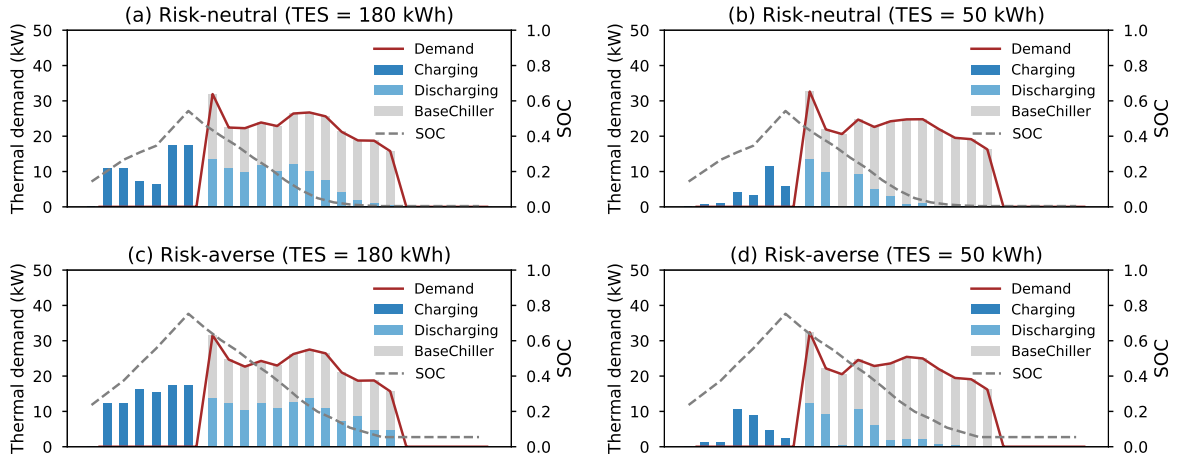

Figure 4: Comparison of detailed cooling operation of Building 1 (June 5th).

6.2.1. Building portfolio without PV generation

Figure 5 shows the results of optimal TES sizing for building portfolios without having any PV generation on site. Across all of the cases, we observed the same pattern that the optimal TES size for each building was different due to their diverse characteristics and customer preferences. The customer preferences had a fairly large influence on the optimal TES sizing among the buildings. By estimating the ratio of the participation of Building 1 (B1), Building 2 (B2), and Building 3 (B3), we see that B1:B2:B3 = 1:1.5:1.25. Accordingly, B2 showed the highest willingness to participate in the DR program and it resulted in the largest TES sizing, while the lower level of participation from B1 resulted in the smallest TES size among the portfolio. This seems logical, since more customer participation and higher TES utilization require larger TES capacity.

Among the different control cases, the risk-averse perspective resulted in TES sizes that were within a few percent of the perfect information case for B2 and B3. For B1 the risk-averse size was 12.6% larger. The deterministic case resulted in the lowest TES sizes for all buildings, and the TES sizing of the risk-neutral case was designed between deterministic and risk-averse cases. The expected demand on the design day for the deterministic and risk-neutral frameworks was lower than the actual building demand, thus, the optimal capacities for these cases were relatively smaller than the perfect information case. On the other hand, the risk-averse case could see that larger TES sizing would be valuable to store additional energy and avoid losses.

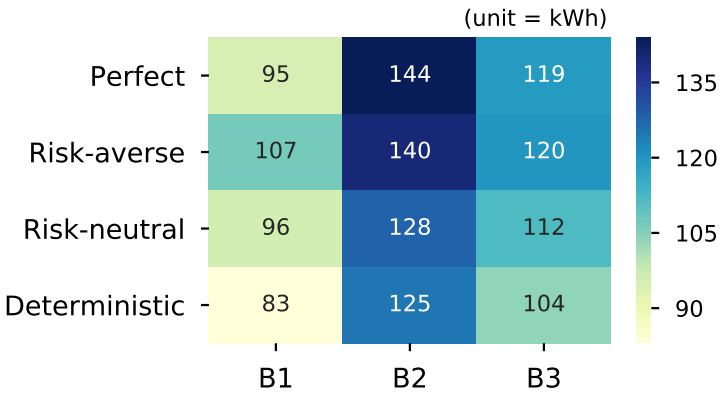

Figure 5: Comparison of Optimal TES sizing.

Table 2: Comparison of peak savings and TES utilization for the building portfolio without PV.

Case	TES utilization (kWh)	Peak (kW)	Peak saving (%)
Deterministic	588.2	33.3	23.3
Risk-neutral	590.1	32.8	24.4
Risk-averse	716.7	31.6	27.2
Perfect	528.4	34.1	21.4
Baseline (No TES)	0	43.4	0

Table 3: Comparison of total costs for the building portfolio without PV.

Case	Operation ($)	Peak penalty ($)	Total costs ($)	Cost savings (%)
Deterministic	53.4	7.2	60.6	33.6
Risk-neutral	52.7	7.0	59.7	34.5
Risk-averse	52.4	4.3	56.7	37.8
Perfect	51.1	6.9	58.0	36.4
Baseline (No TES)	58.6	32.6	91.2	0

Table 2 summarizes the comparison in terms of TES utilization and peak demand. Then, we estimated the peak savings compared to a baseline case without TES. TES utilization was calculated by the sum of charging and discharging energy. It was found that the risk-averse controller utilized TES the most to meet the cooling demand. The risk-averse controller was able to discharge more energy when it was needed due to its tendency to charge and store more energy. Correspondingly, compared to the baseline case, it was able to save around 27.2% of peak power, which is followed by peak savings of the risk-neutral case and the deterministic case. The peak demand savings of the risk-averse controller was 2.8 percentage points higher than the risk-neutral case.

Table 3 shows the comparison in terms of operating cost, peak penalty, total costs, and cost savings. It was observed that the risk-averse control strategy could save costs over deterministic and risk-neutral cases, and the factor affected the most on the cost reduction was the penalty charges. The risk-averse case could save 92.7% of peak penalty charges compared to the deterministic case by discharging enough energy to meet the peak demand limit. Overall, it was determined that risk-averse approach resulted in total cost savings that were 4.2 and 3.3 percentage points higher than deterministic and risk-neutral cases, respectively.

The detailed cooling operation with TES control strategies for Building 1 is illustrated in Figure 6. Each subfigure of Figure 6 represent the operation of each controller case (e.g., deterministic, risk-neutral, risk-averse, and perfect information). The main operating characteristics are highly related to its level of information and TES sizing. For example, the charging strategy (blue bar) of the deterministic case is followed by the expected demand (red dashed line). By checking the state of charge of TES (grey dashed line), the SOC goes above 80-90%. However, the TES size optimized for the deterministic case was 22.7% smaller than the risk-averse case. Thus, although the SOCs are similar, different quantities of energy are stored by each system. Comparing the amount of charging with the blue bar in the figures, the deterministic case charged relatively small amount of energy on the morning of June 5th and it ran out of thermal energy (sky-blue bar) to meet the peak limit in the afternoon. The risk-neutral case was able to utilize more information than the deterministic case, however, it showed a similar operating pattern. For the risk-averse control strategy, it tended to charge more each day so that it could discharge to avoid the peak charge on June 5th even using the energy stored in the previous day. Perfect information case used 1-day perfect forecast information, thus it charged the required amount and discharged the most till the end of the operation. Unlike the operating characteristic of perfect information, the risk-averse case could benefit from the previously-stored energy on June 5th and 9th.

Figure 7 describes the total results in terms of actual power, surplus, and accumulated costs. The first subfigure represents the actual power for each case. The second subfigure shows the hourly surplus

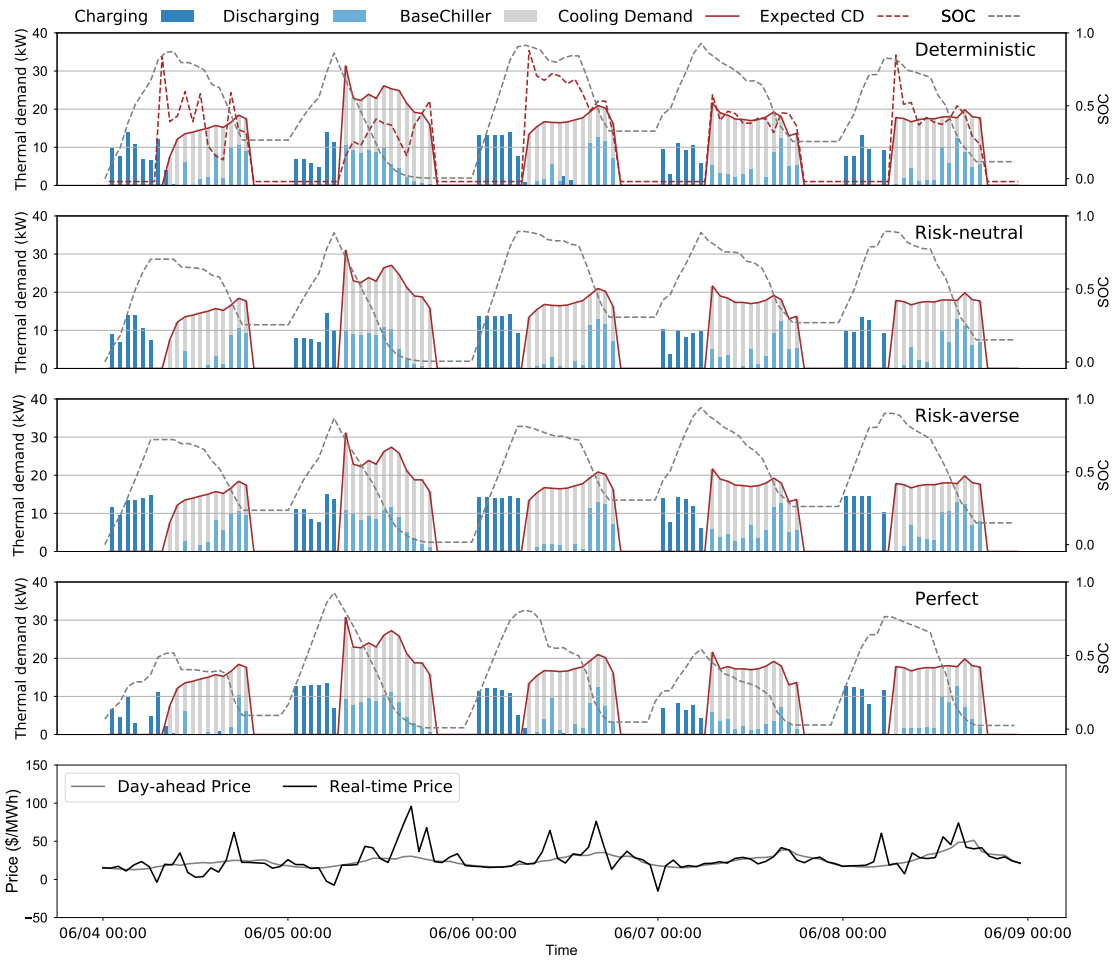

Figure 6: Comparison of detailed cooling operation of Building 1 (June 4th - 8th).

and positive value denotes costs while a negative value means profit. The third subfigure illustrates the aggregated costs over days and the last subfigure shows the day-ahead and real-time power prices.

On June 5th, the original aggregated building demand (grey dashed line) was higher than the other days and peak limit, thus, it was required to operate TES to shave the peak demand. It was found that the risk-averse case (red solid line) was able to avoid the expensive peak penalty charges by discharging fully, similar to the perfect information case. The risk-averse case was successful in that it had lower operating costs by avoiding expensive peak penalty charges on that day. As observed in the second subfigure, all cases except for the risk-averse and perfect information cases had high financial loss on June 5th due to the spike in power price and unexpected high demand. Even though the deterministic case (green solid line) and risk-neutral case (blue solid line) were only slightly above the peak limit, it resulted in expensive charges. In the third subfigure, we can recognize that the accumulated costs for deterministic and risk-neutral cases jumped up over the risk-averse and perfect information cases based on June 5th. The other interesting finding is that the risk-averse case can have lower total costs over the perfect information case since we used a one day perfect forecast and planning horizon. The perfect information case essentially optimizes resource utilizing within the 24-hour period, while the more conservative nature of the risk-averse controller caused it to accumulate some excess storage from previous days that proved beneficial when more extreme scenarios materialized during real-time operations. Thus, the risk-averse perspective may also be able to adjust for some shortsightedness of the controller. Overall, it was determined that the value of the risk-

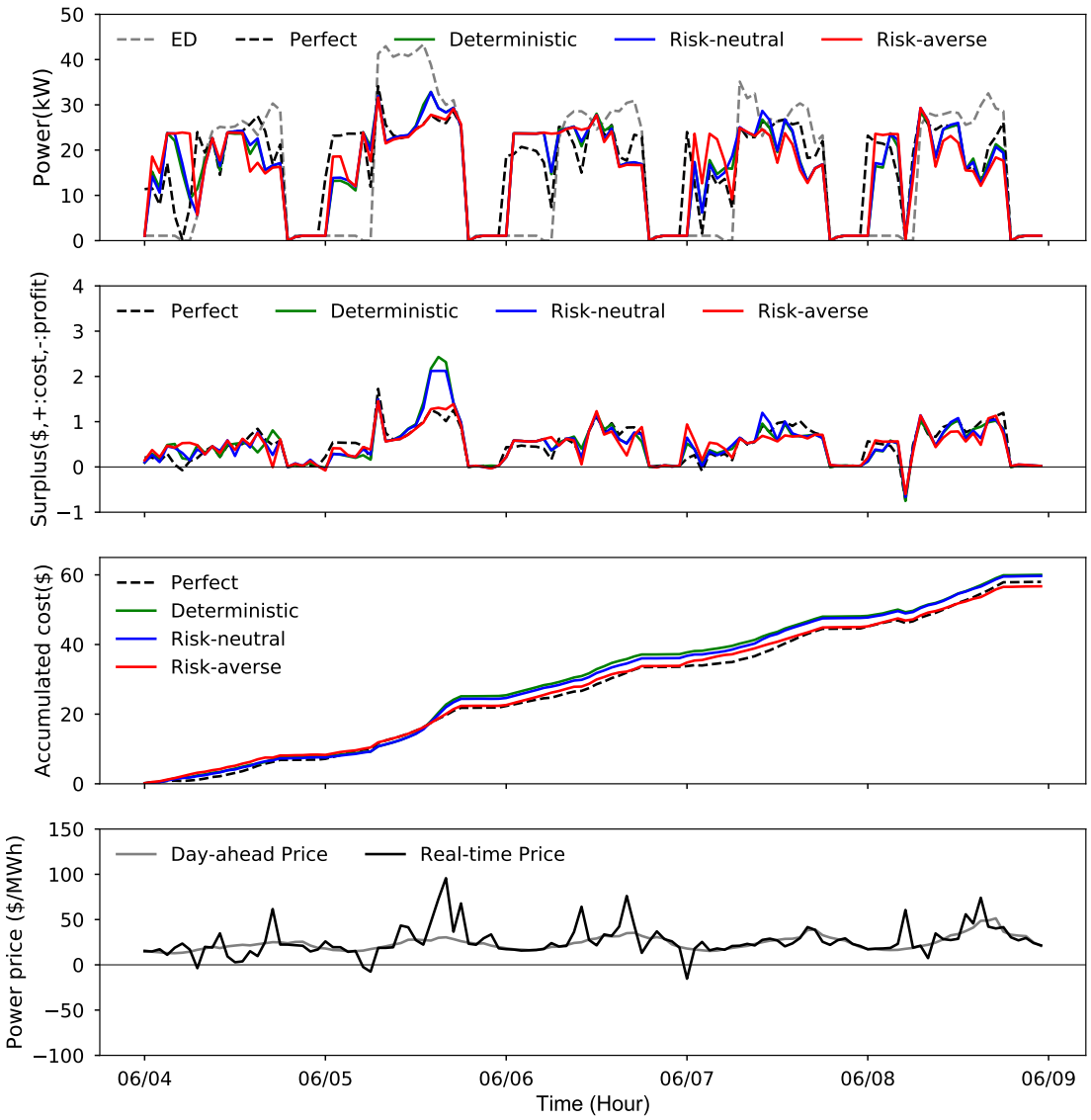

Figure 7: Comparison of actual power, surplus, and aggregated costs over June 4th through 8th.

averse controller was maximized when not only the building demand was unexpectedly high but also when the real-time power prices were extremely volatile.

6.2.2. Buildings portfolio with PV generation

Figure 8 shows the results of optimal TES sizing for building portfolios with PV panels on site. Similar to the results for the building portfolio without PV generation observed in Figure 5, the optimal TES sizing was determined by the building operational characteristics, and the capacities were highly related to the ratio of their participation. Unlike the previous solutions, though, the overall optimal TES capacities were around 20 - 30% lower as it utilizes the power generated from the PV to help reduce demand and costs.

Among the control cases, the risk-averse controller had the largest TES sizing solutions considering financial loss that could come in scenarios where solar PV output is low and building demand is high. Interestingly, the risk-neutral case designed the smallest TES system, thus, it is expected to have a larger performance gap between the risk-neutral and risk-averse cases due to differences in TES utilization.

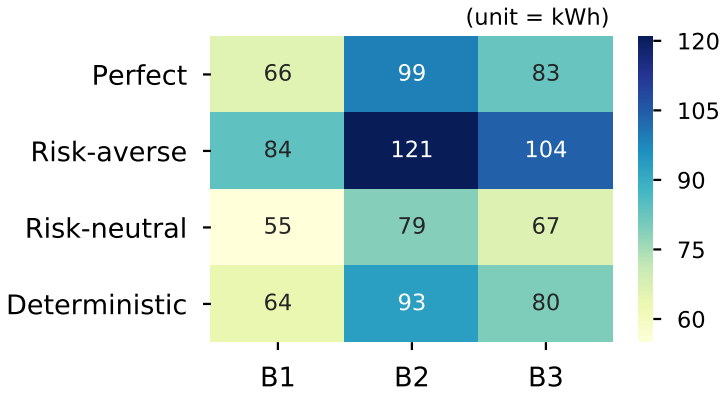

Figure 8: Comparison of optimal TES sizing for the portfolio with PV.

Figure 9 represents the power generated from one PV panel and the electric demand deducted by PV power during the simulation days. In this work, we used the PV panel rated at 250 W_{dc} and assumed that each building installed 50 panels to support its demand. The first subfigure shows the power generation (green solid line) during the simulation period. It varied within its capacity, and we observed that the produced power was lower than half of the typical output on June 5th due to overcast skies. In reality, PV output can also vary due to shade, dust, disconnected components, malfunctions, etc., adding to the potential uncertainty in output. The second subfigure illustrates the aggregated original electric demand

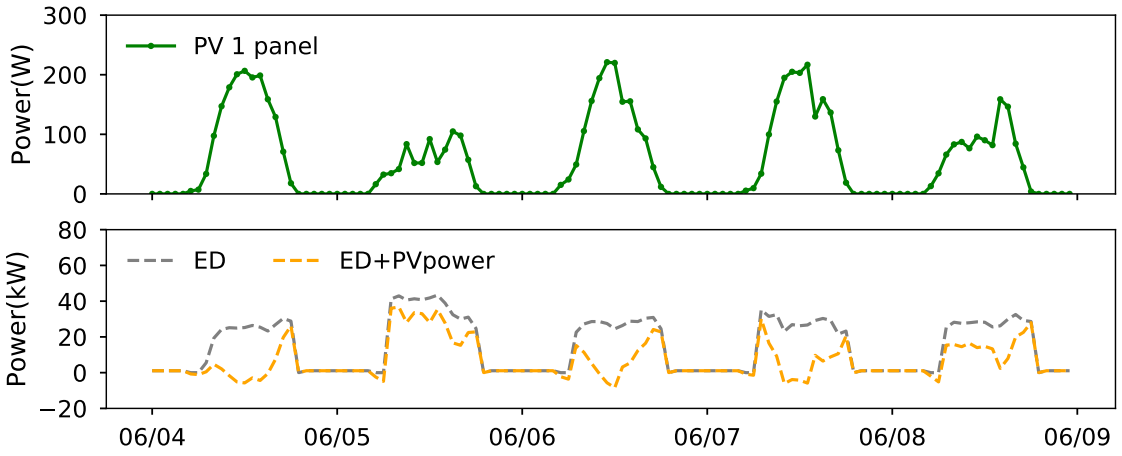

Figure 9: Electric demand with PV power generation.

(grey dashed line) and the one deducted by the power generated from PV panels (yellow dashed line). It was observed that the building could reach net zero load during certain times of the day due to the PV power, however, only a fraction of the building demand could be met by PV power on June 5th.

Table 4 summarizes the comparison of results for the entire building portfolios during the simulation period in terms of TES utilization, peak demand, and peak savings with respect to the baseline case (No TES). The risk-averse control case resulted in the lowest peak demand by utilizing TES as much as possible. Compared to the baseline (no TES), it was able to achieve 31.0% peak power savings, which was twice the savings of the risk-neutral case and deterministic case. Moreover, the risk-neutral case had about 18.5% more TES utilization than deterministic case, even though the TES sizes were about 15% smaller. With this observation, we can suggest that the deterministic optimal sizing and dispatch are not ideal in practice.

Table 4: Comparison of peak saving and TES utilization for building portfolios with PV.

Case	TES utilization (kWh)	Peak (kW)	Peak saving (%)
Deterministic	553.6	31.4	14.4
Risk-neutral	632.3	31.0	15.5
Risk-averse	701.0	25.3	31.0
Perfect	538.8	33.2	9.5
Baseline (No TES)	0	36.7	0

Table 5: Comparison of total costs for building portfolios with PV.

Case	Operation ($)	Peak penalty ($)	Total costs ($)	Cost savings (%)
Deterministic	25.5	9.1	34.6	33.3
Risk-neutral	24.0	8.5	32.5	37.4
Risk-averse	24.8	5.2	30.0	42.2
Perfect	22.7	8.9	31.6	39.1
Baseline (No TES)	27.9	24.0	51.9	0

Table 5 shows the comparison for building portfolios in terms of total costs and cost savings. The risk-averse approach resulted in total cost savings that were 8.9 and 4.8 percentage points higher than the deterministic and risk-neutral cases, respectively. Moreover, the risk-averse case with PV generation had 4.4 percentage points more savings over the risk-averse building portfolios without PV generation.

The detailed TES control strategies for Building 1 with PV generation are illustrated in Figure 10. Unlike the previous TES operation observed in Figure 6, the results showed many dynamic operating characteristics as it charges during the daytime. Especially, the risk-averse controller decided to charge as much when it was available to be prepared for the extreme scenarios.

Figure 11 visualizes the results with actual power, surplus, and accumulated costs. As only a fraction of the building electric demand was met by PV power on June 5th, the performance among the controllers varied significantly due to their different handling of this somewhat atypical low output scenario. Since the risk-averse control strategy considered the potentially expensive scenarios when decision making, it could absorb the low PV output by discharging more thermal energy. However, the deterministic and risk-neutral cases did not charge enough, thus, they ended up incurring costly peak penalty charges as observed in the second subfigure. If we take a look at the aggregated costs in the third subfigure, the financial gap is large, and it remained until the end of the simulation period. Therefore, it was confirmed that the aggregator can benefit a lot from the risk-averse controller when the more extreme conditions occur (e.g., high building demand, low PV generation, volatile power prices, etc.) and the values can be increased when more volatile and unexpected situations are expected. Another interesting finding is that there are similar power profile on June 6th compared to the results for building portfolios without PV generation. This is because all the cases decided to charge more however the maximum charging amount is limited due to lower peak demand limit for the building portfolios with PV generation.

7. Conclusion and discussion

This work presented an uncertainty- and risk-aware transactive energy control framework for a building portfolio integrating thermal energy storage and PV systems. We formulated the risk-averse control framework by incorporating conditional value-at-risk into a scenario-based two-stage stochastic optimization to help avoid costly decision errors that lead to substantial financial loss at the tail of cost distribution. The risk-neutral framework tends to emphasize scenarios near the mean and cannot adequately contend with more extreme realizations. Notably, this framework can react to more dynamics in building demand

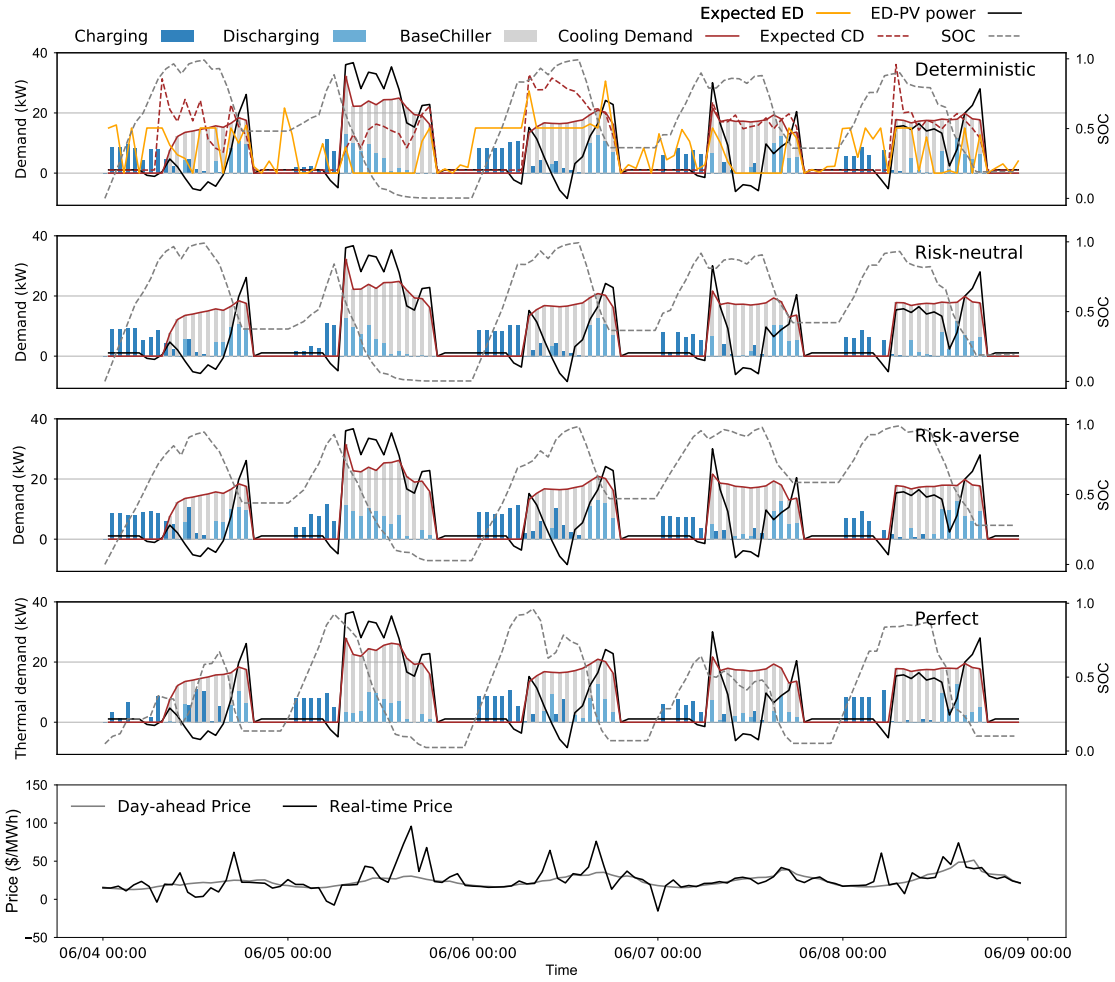

Figure 10: Comparison of detailed cooling operation (June 4th - 8th).

and power prices. Two case studies were performed to quantify the capabilities of risk-averse controllers depending on the building TES capacities and building load variations.

To maximize the performance of the risk-averse controller, we explored the operating characteristics related to the TES sizing. From the results, the risk-averse case could not perform well to meet the peak limit if the TES was too small. The peak penalty charges increased significantly with the smaller TES capacity. Therefore, it was demonstrated that the performance of the stochastic framework is highly related to the TES sizing depending on the risk-cognizant level.

Based on the optimal TES sizing solution for building portfolio, the risk-averse case had the largest capacity to store extra thermal energy for emergency situations. Also, it was related to the customer's participation in the DR program. Therefore, the building customers having higher participation were determined to install a bigger TES size. Then, we performed case studies to highlight the benefits of the risk-averse controller with more variability.

Our numerical studies demonstrated that the risk-averse controller is capable to adapt to the dynamic changes in building demand and power prices as it charges more each day and can discharge the stored energy from previous days to avoid peak demand and volatile power prices. From the peaking savings and cost reduction, the risk-averse stochastic optimization model was successful in mitigating financial risk when more variability and uncertainties were included in building demand with respect to the capabilities

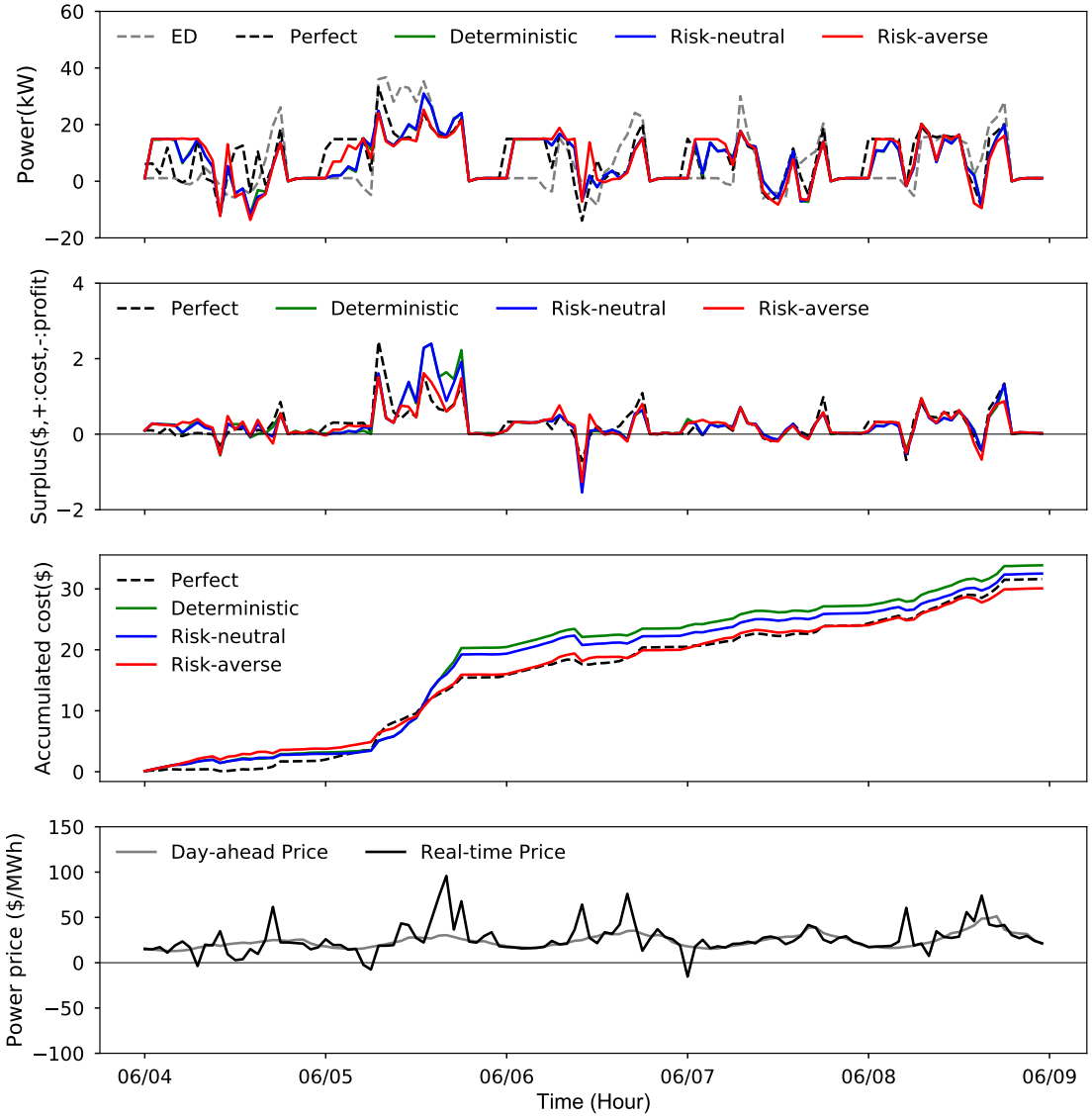

Figure 11: Comparison of actual power, surplus, and aggregated costs over June 4th through 8th.

of the deterministic controller. This work provides comprehensive information for the demand response aggregators to have the intelligence to predict demand patterns as well as potential financial loss This study also highlights the opportunities to turn buildings into already deployed storage options for the grid to balance both peaks and valleys of demand.

Bibliography

[1] Connor P, Axon C, Xenias D, Balta-Ozkan N. Sources of risk and uncertainty in uk smart grid deployment: An expert stakeholder analysis. Energy 2018;161. doi:10.1016/j.energy.2018.07.115.

[2] Jankauskas V, Rudzkis P, Kanopka A. Risk factors for stakeholders in renewable energy investments. Energetika 2014;60. doi:10.6001/energetika.v60i2.2935.

[3] Enrico Z, Terje A. Uncertainties in smart grids behavior and modeling: What are the risks and vulnerabilities? how to analyze them? 2011. doi:10.1016/j.enpol.2011.07.030.

[4] Panteli M, Mancarella P. Influence of extreme weather and climate change on the resilience of power systems: Impacts and possible mitigation strategies. Electric Power Systems Research 2015;127. doi:10.1016/j.epsr.2015.06.012.
[5] Jufri F, Widiputra V, Jung J. State-of-the-art review on power grid resilience to extreme weather events: Definitions, frameworks, quantitative assessment methodologies, and enhancement strategies. Applied Energy 2019;239:1049–65. doi:10.1016/j.apenergy.2019.02.017.
[6] Moazami A, Carlucci S, Nik V, Geving S. Towards climate robust buildings: an innovative method for designing buildings with robust energy performance under climate change. Energy and Buildings 2019;:109378doi:10.1016/j.enbuild.2019.109378.
[7] Yu MG, Pavlak GS. Two-stage stochastic planning for control of building thermal energy storage portfolios with transactive controls. In: 2020 American Control Conference (ACC). 2020, p. 2339–44. doi:10.23919/ACC45564.2020.9147670.
[8] Yu MG, Pavlak GS. Assessing the performance of uncertainty-aware transactive controls for building thermal energy storage systems. Applied Energy 2021;282:116103. URL: http://www.sciencedirect.com/science/article/pii/S0306261920315233. doi:https://doi.org/10.1016/j.apenergy.2020.116103.
[9] Díaz P, Adler C, Patt A. Do stakeholders' perspectives on renewable energy infrastructure pose a risk to energy policy implementation? a case of a hydropower plant in switzerland. Energy Policy 2017;Volume 108:21–8. doi:10.1016/j.enpol.2017.05.033.
[10] Sun Y, Li Y, Cai Bf, Li Q. Comparing the explicit and implicit attitudes of energy stakeholders and the public towards carbon capture and storage. Journal of Cleaner Production 2020;254:120051. doi:10.1016/j.jclepro.2020.120051.
[11] Wagemann B, Manetsgruber D. Risk management for mini-grid deployment in rural areas. Energy Procedia 2016;103:106–10. doi:10.1016/j.egypro.2016.11.257.
[12] Hussain A, Bui VH, Kim HM. Robust optimization-based scheduling of multi-microgrids considering uncertainties. Energies 2016;9:1–21. doi:10.3390/en9040278.
[13] Perera A, Nik V, Chen D, Scartezzini J, Hong T. Quantifying the impacts of climate change and extreme climate events on energy systems. Nature Energy 2020;5:150–159. doi:10.1038/s41560-020-0558-0.
[14] Wang Y, Chen C, Wang J, Baldick R. Research on resilience of power systems under natural disasters—a review. IEEE Transactions on Power Systems 2015;31:1–10. doi:10.1109/TPWRS.2015.2429656.
[15] Zhai C, Zhang H, Xiao G, Pan TC. A model predictive approach to protect power systems against cascading blackouts. International Journal of Electrical Power and Energy Systems 2019;doi:10.1016/j.ijepes.2019.05.029.
[16] Vahedipour-Dahraie M, Rashidi H, Najafi H, Anvari-Moghaddam A, Guerrero J. Stochastic security and risk-constrained scheduling for an autonomous microgrid with demand response and renewable energy resources. IET Renewable Power Generation 2017;11. doi:10.1049/iet-rpg.2017.0168.
[17] Vahedipour-Dahraie M, Rashidi H, Anvari-Moghaddam A. Risk-constrained stochastic scheduling of a grid-connected hybrid microgrid with variable wind power generation. Electronics 2019;8:1–17. doi:10.3390/electronics8050577.
[18] Yin PY, Cheng CY, Chen HM, Wu TH. Risk-aware optimal planning for a hybrid wind-solar farm. Renewable Energy 2020;157:290–302. URL: https://www.sciencedirect.com/science/article/pii/S0960148120307011. doi:https://doi.org/10.1016/j.renene.2020.05.003.
[19] Ali M, Safdarian A, Lehtonen M. Risk-constrained framework for residential storage space heating load management. Electric Power Systems Research 2015;119:432–8. URL: https://www.sciencedirect.com/science/article/pii/S0378779614003952. doi:https://doi.org/10.1016/j.epsr.2014.10.024.
[20] Tian MW, Yan SR, Tian XX, Kazemi M, Nojavan S, Jermsittiparsert K. Risk-involved stochastic scheduling of plug-in electric vehicles aggregator in day-ahead and reserve markets using downside risk constraints method. Sustainable Cities and Society 2020;:102051doi:10.1016/j.scs.2020.102051.
[21] Donglin Zheng Lijun Yu LW. A techno-economic-risk decision-making methodology for large-scale building energy efficiency retrofit using monte carlo simulation. Energy 2019;:116169doi:10.1016/j.energy.2019.116169.
[22] Tavakoli M, Shokridehaki F, Funsho Akorede M, Marzband M, Vechiu I, Pouresmaeil E. Cvar-based energy management scheme for optimal resilience and operational cost in commercial building microgrids. International Journal of Electrical Power and Energy Systems 2018;100:1–9. doi:10.1016/j.ijepes.2018.02.022.
[23] Golpîra H, Khan S. A multi-objective risk-based robust optimization approach to energy management in smart residential buildings under combined demand and supply uncertainty. Energy 2019;170. doi:10.1016/j.energy.2018.12.185.
[24] Cano EL, Moguerza J, Alonso-Ayuso A. A multi-stage stochastic optimization model for energy systems planning and risk management. Energy and Buildings 2015;110. doi:10.1016/j.enbuild.2015.10.020.
[25] Tavakoli M, Shokridehaki F, Marzband M, Godina R, Pouresmaeil E. A two stage hierarchical control approach for the optimal energy management in commercial building microgrids based on local wind power and pevs. Sustainable Cities and Society 2018;41. doi:10.1016/j.scs.2018.05.035.
[26] Dolatabadi A, Mohammadi-ivatloo B. Stochastic risk-constrained scheduling of smart energy hub in the presence of wind power and demand response. Applied Thermal Engineering 2017;123. doi:10.1016/j.applthermaleng.2017.05.069.
[27] Jadidbonab M, Babaei E, Mohammadi-ivatloo B. Cvar-constrained scheduling strategy for smart multi carrier energy hub considering demand response and compressed air energy storage. Energy 2019;174. doi:10.1016/j.energy.2019.02.048.
[28] Xu X, Hu W, Liu W, Du Y, Huang R, Huang Q, et al. Look-ahead risk-constrained scheduling for an energy hub integrated with renewable energy. Applied Energy 2021;297:117109. URL: https://www.sciencedirect.com/science/article/pii/S0306261921005535. doi:https://doi.org/10.1016/j.apenergy.2021.117109.
[29] Ghaffarpour R. Optimal sizing, scheduling and building structure strategies for a risk-averse isolated hybrid energy system in kish island. Energy and Buildings 2020;:110008doi:10.1016/j.enbuild.2020.110008.
[30] Habibifar R, Lekvan A, Ehsan M. A risk-constrained decision support tool for ev aggregators participating in energy and frequency regulation markets. Electric Power Systems Research 2020;185:106367. doi:10.1016/j.epsr.2020.106367.

[31] Rashidi H, Vahedipour-Dahraie M, Najafi H, Anvari-Moghaddam A, Guerrero J. A stochastic bi-level scheduling approach for the participation of ev aggregators in competitive electricity markets. Applied Sciences 2017;7:1100. doi:10.3390/app7101100.
[32] Mansour-lakouraj Mohammad SM. Comprehensive analysis of risk-based energy management for dependent micro-grid under normal and emergency operations. Energy 2019;171. doi:10.1016/j.energy.2019.01.055.
[33] Ghose T, Pandey H, Gadam K. Risk assessment of microgrid aggregators considering demand response and uncertain renewable energy sources. Journal of Modern Power Systems and Clean Energy 2019;doi:10.1007/s40565-019-0513-x.
[34] Nguyen DT, Le LB. Risk-constrained profit maximization for microgrid aggregators with demand response. IEEE Transactions on Smart Grid 2015;6(1):135–46. doi:10.1109/TSG.2014.2346024.
[35] Vahedipour-Dahraie M, Rashidizadeh-Kermani H, Anvari-Moghaddam A, Guerrero JM. Stochastic risk-constrained scheduling of renewable-powered autonomous microgrids with demand response actions: Reliability and economic implications. IEEE Transactions on Industry Applications 2020;56(2):1882–95. doi:10.1109/TIA.2019.2959549.
[36] Rashidi H, Vahedipour-Dahraie M, Anvari-Moghaddam A, Guerrero J. Stochastic risk-constrained decision-making approach for a retailer in a competitive environment with flexible demand side resources. International Transactions on Electrical Energy Systems 2018;doi:10.1002/etep.2719.
[37] Rashidi H, Vahedipour-Dahraie M, Shafie-khah M, Catalão J. Stochastic programming model for scheduling demand response aggregators considering uncertain market prices and demands. International Journal of Electrical Power and Energy Systems 2019;113:528–538. doi:10.1016/j.ijepes.2019.05.072.
[38] Henze G, Felsmann C, Knabe G. Evaluation of optimal control for active and passive building thermal storage. International Journal of Thermal Sciences 2004;43:173–83. doi:10.1016/j.ijthermalsci.2003.06.001.
[39] Luetkepohl H. The New Introduction to Multiple Time Series Analysis. 2005. ISBN 978-3-540-40172-8. doi:10.1007/978-3-540-27752-1.
[40] Seabold S, Perktold J. statsmodels: Econometric and statistical modeling with python. In: 9th Python in Science Conference. 2010,.
[41] Wan W. Algorithms for operation of power systems: Risk, uncertainty, discreteness, and nonconvexity. Ph.D. thesis; 2019.
[42] ApS M. MOSEK Optimizer API for Python 9.0.105; 2021. URL: https://docs.mosek.com/9.0/pythonfusion.pdf.